

A Journal of the Gesellschaft Deutscher Chemiker

Angewandte Chemie

GDCh

International Edition

www.angewandte.org

Accepted Article

Title: Screening Heteroatom Configurations for Reversible Sloping Capacity Promises High-Power Na-Ion Batteries

Authors: Fei Xie, Yaoshen Niu, Qiangqiang Zhang, Zhenyu Guo, Zilin Hu, Quan Zhou, Zhen Xu, Yuqi Li, Ruiting Yan, Yaxiang Lu, Maria-Magdalena Titirici, and Yong-Sheng Hu

This manuscript has been accepted after peer review and appears as an Accepted Article online prior to editing, proofing, and formal publication of the final Version of Record (VoR). The VoR will be published online in Early View as soon as possible and may be different to this Accepted Article as a result of editing. Readers should obtain the VoR from the journal website shown below when it is published to ensure accuracy of information. The authors are responsible for the content of this Accepted Article.

To be cited as: *Angew. Chem. Int. Ed.* **2022**, e202116394

Link to VoR: <https://doi.org/10.1002/anie.202116394>

Screening Heteroatom Configurations for Reversible Sloping Capacity Promises High-Power Na-Ion Batteries

Fei Xie,^[a] Yaoshen Niu,^[a,b] Qiangqiang Zhang,^[a,b] Zhenyu Guo,^[c] Zilin Hu,^[a,b] Quan Zhou,^[a] Zhen Xu,^[c] Yuqi Li,^[a,b] Ruiting Yan,^[d] Yaxiang Lu,^{*[a]} Maria-Magdalena Titirici,^[c] and Yong-Sheng Hu^{*[a,b]}

- [a] Dr. F. Xie, Y. Niu, Dr. Q. Zhang, Z. Hu, Dr. Q. Zhou, Y. Li, Prof. Y. Lu, Prof. Y.-S. Hu
Key Laboratory for Renewable Energy, Beijing Key Laboratory for New Energy Materials and Devices, Beijing National Laboratory for Condensed Matter Physics, Institute of Physics, Chinese Academy of Sciences
Beijing, 100190, China
E-mail: yxlu@iphy.ac.cn; yshu@iphy.ac.cn
- [b] Y. Niu, Dr. Q. Zhang, Z. Hu, Y. Li, Prof. Y.-S. Hu
College of Materials Science and Optoelectronics Technology, University of Chinese Academy of Sciences
Beijing, 100049, China
- [c] Z. Guo, Z. Xu, Prof. M.-M. Titirici
Department of Chemical Engineering, Imperial College London
London, SW7 2AZ, UK
- [d] Dr. R. Yan
Central Research Institute, Huawei Technologies, Shenzhen, 518129, China

Supporting information for this article is given via a link at the end of the document.

Abstract: Heteroatom doping has been proved to effectively enhance the sloping capacity, nevertheless, the high sloping capacity almost encounters a conflict with the disappointing initial Coulombic efficiency (ICE). Herein, we propose a heteroatom configuration screening strategy by introducing a secondary carbonization process for the phosphate-treated carbons to remove the irreversible heteroatom configurations but with the reversible ones and free radicals remained, achieving a simultaneity between the high sloping capacity and ICE (~250 mAh g⁻¹ and 80%). The Na storage mechanism was also studied based on this “slope-dominated” carbon to revealed the reason of the absence of the plateau. This work could inspire to distinguish and filter the irreversible heteroatom configurations and facilitate the future design of practical “slope-dominated” carbon anodes towards high-power Na-ion batteries.

Introduction

Na-ion batteries (NIBs) as an alternative to lead-acid batteries and a supplement to Li-ion batteries (LIBs), have been earning more and more attention with the increased demand of renewable energy today owing to the huge abundance and wide distribution of Na resources in the world.^[1–4] This distinct advantage promises the applications of NIBs in large-scale energy storage such as smart power grids/stations, 5G base

stations and data centers, *etc.* In the past decades, pursuing high energy density through improving the specific capacity of electrode materials had always been the goal of research. Nevertheless, with the need of various application scenarios, power density and safety properties also arouse the concern and are regarded as important as the energy density.

From the view of anode side, disordered carbons are generally believed as the most promising commercial anode choices for NIBs, and great contributions have been made to push the Na storage capacity more than 400 mAh g⁻¹.^[5–9] It is known that the typical galvanostatic discharge/charge curves of disordered carbon anodes consist a high-potential sloping region (above ~0.1 V vs. Na⁺/Na) and a low-potential plateau region (0–0.1 V vs. Na⁺/Na), where most of the capacity improvement comes from the plateaus. However, the long plateau is the diffusion-controlled process and suffers from slower kinetics to restrain the rate performance, meanwhile, the low voltage close to the Na plating may lead to safety issues particularly at high rates.^[10,11] On the contrary, the sloping region has faster kinetics and better rate capability, while the higher average potential is also able to diminish the Na plating during cycling.^[12,13] Thereby, developing “slope-dominated” carbons (with dominated sloping region without obvious plateau in the discharge/charge profiles) is regaining researchers’ attention for producing high-power and safe NIBs to fulfil the requirements of large-scale energy storage markets.

It has been widely investigated that the heteroatom doping (N, P, O, etc.) is able to promote the pseudocapacitive adsorption of Na^+ ions in the parent carbons and effectively enhance the sloping capacity.^[14,15] Nevertheless, the obtained “slope-dominated” carbons usually encounter the conflict of high sloping capacity and low initial Coulombic efficiency (ICE) in normal ester-based electrolytes.^[16–18] An important reason is the introduced heteroatom configurations may cause extra reversible and irreversible capacities at the same time.^[19–21] Despite the low ICE is reported to be easily addressed by using ether-based electrolytes,^[22–24] it is still limiting in the full cell for future commercialization since the ether-based electrolytes are higher-cost and not oxidatively stable enough at high voltage.^[25] Our group has obtained a balanced performance between the sloping capacity and ICE from a kind of pitch via a low-temperature carbonization strategy owing to the abundant oxygen contents and defects,^[26] but the good performance is somewhat dependent on the intrinsic structures based on the precursor selection, while the deep understanding of why this balance can be realized is still unclear. Therefore, achieving the simultaneity between the high sloping capacity and ICE in ester-based electrolytes is still a significant and challenging task, where one urgent goal is to distinguish and filter the heteroatom configurations for reversible Na adsorption from the view of electrode surface chemistry.

Herein, we propose a heteroatom configuration screening strategy to simultaneously achieve the high sloping capacity and ICE in normal ester electrolytes based on both low-cost carbon and heteroatom precursors (petroleum residues and NaH_2PO_4). Through a secondary carbonization process upon the removal of the Na-containing compounds after the initial annealing, though the total percentage of the heteroatoms decreased, some specific heteroatom configurations of $\text{C}=\text{O}$ and $\text{PO}_2^{\cdot-}/\text{PO}_4^{3-}$ as well as free radicals were maintained or improved, which resulted in the endured high sloping capacity of $\sim 250 \text{ mAh g}^{-1}$. On the other hand, some configurations with more irreversible capacities including $\text{C}-\text{O}$ and $\text{PO}_3^{\cdot-}$ were diminished by the secondary carbonization, leading to a recovered ICE to 80%. Moreover, the Na storage mechanisms of this “slope-dominated” carbon were also systematically studied, finding that the diffusion-controlled process at the low potential region, but the too small nanopore sizes lead to unsatisfied Na accommodation and the absence of the plateau. The resulting “slope-dominated” carbon anodes were also paired with different cathodes to optimize the full cell performance. The excellent rate performance (124 mAh g^{-1} even at a high rate of 20C) and capacity retention (86% after 1000 cycles and 72% after 2000 cycles at 3C) suggest the great potential of practical “slope-dominated” carbon anodes with both high sloping capacity and ICE towards high-power NIBs inspired by distinguishing and filtering the irreversible heteroatom configurations.

Results and Discussion

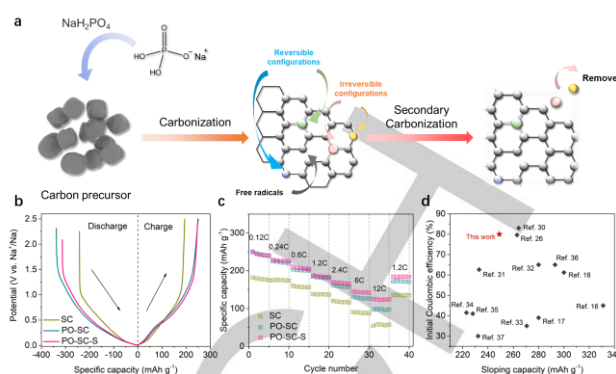


Figure 1. (a) Schematic illustration of the heteroatom configurations screening strategy. (b-c) Initial galvanostatic discharge/charge profiles and rate performance of the SC, PO-SC and PO-SC-S. (d) A comparison of the sloping capacity and ICE between the PO-SC-S and reported values from literatures.

The scheme of the heteroatom configurations screening strategy is shown in Figure 1a. A low-cost petroleum residue precursor with relatively low intrinsic heteroatom contents was used as carbon precursor to mix with the low-cost P/O source of NaH_2PO_4 with the optimized mass ratio of 1:4. The mixture was then carbonized at 800°C with subsequent washing by deionized water to remove the Na-containing compounds. The obtained P/O co-doped sample is denoted as PO-SC, while the pristine soft carbon from the pure petroleum residues carbonized at 800°C is denoted as SC. For comparison, the petroleum residues were also mixed with NaH_2PO_4 at mass ratios of 1:1 and 1:9 and carbonized at 800°C (denoted as PO-SC-11 and PO-SC-19, respectively). Galvanostatic discharge/charge measurements were performed in half cells first to evaluate the electrochemical performance of the resulting carbons in ester-based electrolyte. As shown in Figure 1b, Figure S1a-b and Table S1, the SC can only deliver an unsatisfied reversible capacity of 194 mAh g^{-1} at 0.12C ($1\text{C}=250 \text{ mA g}^{-1}$) but with a high ICE of 80%, where the capacity is mainly from the sloping region. The addition of the NaH_2PO_4 enhances the sloping capacity as expected, and higher amount of NaH_2PO_4 could lead to higher capacities, which delivers 251 mAh g^{-1} for PO-SC and 267 mAh g^{-1} for PO-SC-19. However, the ICE decreases from 80% to 74% and even 60%, respectively, which is consistent with previous reports.^[19,27,28] This suggests that simply doping heteroatoms is not an effective way to produce practical “slope-dominated” carbons due to the sacrificed ICE, even if the capacity could be effectively increased.

It is known that higher degree of carbonization could optimize the microstructures of carbons, which is able to improve the reversibility.^[21,29] Herein, the PO-SC was carbonized again at 800°C and denoted as PO-SC-S. It is worth noting that some inorganic Na-containing compounds that were introduced by the utilization of NaH_2PO_4 precursor have been removed by deionized water after the first pyrolysis, so the samples undergo first- and second-time carbonization are intrinsically different, making the secondary carbonization process meaningful.

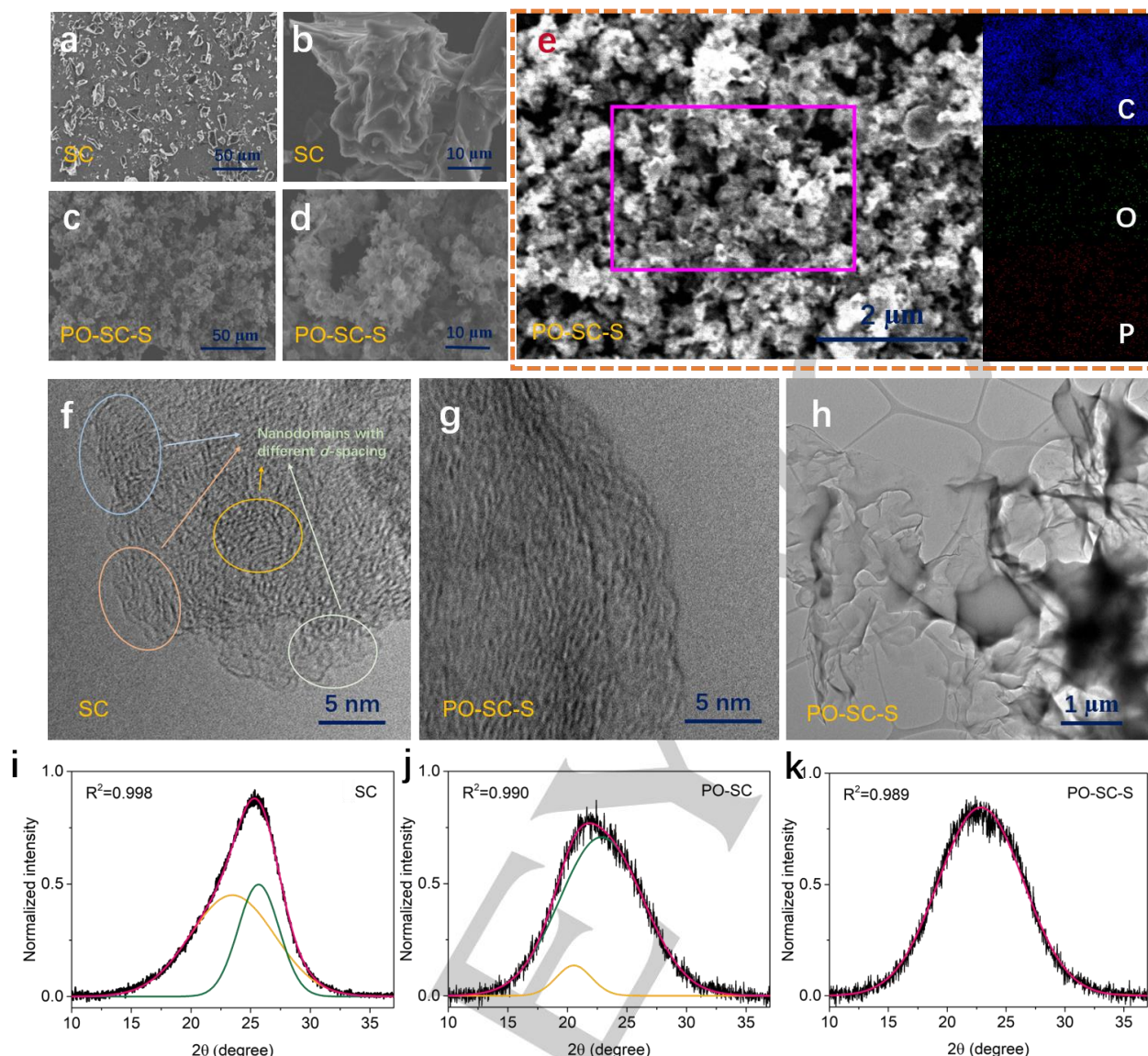


Figure 2. (a-e) SEM images of SC, and PO-SC-S, respectively with the EDX mappings of C, O and P elements. (f-h) TEM images of SC and PO-SC-S, respectively. (i-k) Fittings of XRD (002) peaks of the SC, PO-SC and PO-SC-S, respectively.

It can be seen from Figure 1b that the reversible capacity of PO-SC-S after the secondary carbonization is almost unchanged (249 mAh g^{-1}) compared to the PO-SC, while the ICE recovered to 80%. However, the higher temperature of the secondary carbonization at $1000 \text{ }^\circ\text{C}$ (PO-SC-S1000) led to a lower capacity and ICE (Figure S1a). In addition, the P/O-doped carbons with the enhanced capacity also show lower average voltage than SC, where the PO-SC-S can achieve a high capacity of 200 mAh g^{-1} between 0-1 V (vs. Na^+/Na). Since the nature of the sloping profile has relatively higher working voltage than the plateau, which will unavoidably affect the energy density when assembling full cells. The enhanced capacity and lowered working voltage of PO-SC-S can also offset the energy density in full cells. The rate performance of all the resulting carbons were measured from 0.12C to 12C, and the PO-SC-S exhibits the best rate capability of 249, 229, 211, 187, 170, 145 and 125 mAh g^{-1} at 0.12C, 0.24C, 0.6C, 1.2C, 2.4C, 6C and 12C, respectively among all the samples (Figure 1c and Figure S1c-d). Figure 1d shows the comparison of the reversible capacity and ICE of the PO-SC-S in this work and previous reported "slope-

dominated" carbon anodes at $20\text{-}50 \text{ mA g}^{-1}$ in normal ester-based electrolytes.^[16,17,36,37,18,26,30-35] Although the sloping capacity could be achieved as high as over 300 mAh g^{-1} , most of them deliver extremely disappointing ICE even below 60%, and only very limited materials, including PO-SC-S, can present the balance between the high sloping capacity and ICE.

Why the secondary carbonized carbons can obtain excellent rate performance and achieve both high sloping capacity and ICE? To answer these questions, a series of characterizations were conducted. The scanning electron microscopy (SEM) images of the carbon samples are shown in Figure 2a-d and Figure S2. The particles of SC present as individual big chunks with dense surfaces. With the elevated ratios of the NaH_2PO_4 , the chunks become smaller and are cross-linked together with looser surfaces, which is similar to PO-SC-S after the secondary carbonization process. The diminishment, crosslinking as well as the loose surface of the P/O-doped carbon particles are beneficial to the improvement of Na^+ ions transportation and diffusion, thus enhancing the rate performance (Figure S1c-d).^[38] However, at higher temperature

of the secondary carbonization, the cross-linked particles began to broke and returned to individual chunks (Figure S2g-h), which resulted in the poorer rate capability of PO-SC-S1000. Figure 2e is the SEM image of PO-SC-S with the energy dispersive X-ray (EDX) mappings of C, O and P, showing that the O and P elements are distributed uniformly in the material.

Transmission electron microscopy (TEM) was conducted to observe the local microstructures of the obtained “slope-dominated” carbons. It is found from Figure 2f that there are several nanodomains with turbostratic graphene layers in the SC (circled by different colors), where the interlayer distances are obviously different, suggesting that the SC has a disordered microstructure and its interlayers of the graphitic planes distribute heterogeneously. Meanwhile, the interlayers of the graphitic nanodomains in the PO-SC-S and other P/O-doped samples do not show such strong inhomogeneous distribution like SC (Figure 2g and Figure S3), and the morphology of the PO-SC-S presents as a thin nanosheet (Figure 2h) at lower magnification, which could also facilitate the rate performance.

X-ray diffraction (XRD) results further confirmed the relative more homogeneous distribution of graphene interlayer distances of the P/O-doped carbons. As shown in Figure S4, the (002) peaks at around 23° shift to lower diffraction angles with the increased amount of the NaH_2PO_4 , indicating enlarged average interlayer spacing from 3.51 up to 4.05 Å for PO-SC-S19, while the secondary carbonization decreased the interlayer distances of PO-SC from 3.92 Å to 3.89 Å and 3.59 Å for PO-SC-S and PO-SC-S1000, respectively (Table S2). However, the (002) peak of SC is apparently asymmetric and must be well fitted by two Gaussian peaks (Figure 2i and Figure S5a). With the doping of P and O, the asymmetry of the (002) peaks gradually weakens with the elevated ratios of NaH_2PO_4 , while the peak turns to be symmetric and could be properly fitted by only single Gaussian peak for PO-SC-S after the secondary carbonization at 800 °C (Figure 2j-k and Figure S5b-c). Further increasing the carbonization temperature to 1000 °C made the (002) peak of PO-SC-S1000 become asymmetric again (Figure S5d). The above fitting results suggest that the P/O doping and proper secondary carbonization treatment could optimize the local structures and homogenize the interlayer distances of the turbostratic nanodomains, which is consistent with the TEM images. The uniformly distributed interlayers could decrease the barrier of Na^+ ions transportation and diffusion, which improves the rate performance of PO-SC-S. Furthermore, from the electrochemical impedance spectroscopy (EIS) shown in Figure S6, the semicircles of the PO-SC and PO-SC-S at high-frequency region show much smaller radii compared to that of SC, which also proves the improved rate capabilities.^[39,40] Thus, it could be generally concluded that the cross-linked particles with looser surface as well as the relatively homogeneous distribution of the interlayer spacing facilitate the rate performance of the PO-SC-S.

Commonly, defects, specific surface area and heteroatoms are the most key factors that can affect the sloping capacity and ICE. Thus, Raman spectra were used to first study the defects within the graphitic planes of the resulting carbon samples. The two typical peaks for disordered carbons at around 1340 and 1580 cm^{-1} corresponding to the D- and G-band were fitted by using Lorentz and Breit-Wigner-Fano (BWF) models, respectively (Figure S7).^[41] According to the “three-stage”

Raman models proposed by Ferrari, et al.,^[42–44] as presented in Table S2, for disordered carbons, the intensity ratios of the fitted D- and G-peaks I_D/I_G continuously decrease from 1.03 for SC to 0.97 for PO-SC-19 with the increased amount of NaH_2PO_4 , indicating more defects created in the graphene planes^[38,41,45,46] with the continuous P/O doping. Upon the secondary carbonization, the I_D/I_G slightly declines from 1.00 for PO-SC to 0.99 and 0.98 for PO-SC-S and PO-SC-S1000, respectively, suggesting the defects are increased by the secondary carbonization, which could be attributed to the broken of 6-member carbon rings within the graphene planes upon the decomposition of some heteroatom-containing species.

It is known that disordered microstructures with turbostratic nanodomains and defects can provide abundant Na storage sites to enhance the sloping capacity, but the defects would also trap Na^+ ions to lower the ICE.^[8,29] As expected, with the addition and increasing amount of NaH_2PO_4 , more introduced defects enhance the sloping capacities and reduce the ICEs. However, this is not able to well explain the cases with the secondary carbonization. Meanwhile, the variation of I_D/I_G is relatively slight, implying defect is not the main factor to affect the sloping capacity and ICE. On the other hand, Brunauer–Emmett–Teller (BET) surface areas of the “slope-dominated” carbon samples are all smaller than 15 $\text{m}^2 \text{g}^{-1}$ except PO-SC-19 of $\sim 40 \text{m}^2 \text{g}^{-1}$ based on the N_2 adsorption measurements (Figure S8 and Table S2), thus the surface area-induced electrolyte decomposition and SEI formation may also not be the main influence on the ICE of P/O doped samples except PO-SC-19. Therefore, both defect concentration and BET surface area are not the decisive factors to change the sloping capacity and ICE, which probably correlate to the doped P and O heteroatoms.

Given the above considerations, X-ray photoelectron spectroscopy (XPS) was performed to investigate the P/O heteroatoms and their configurations. As shown in Figure S9 and Figure 3a, the ratio of O increases by twice from 4.14 at.% for SC to 8.99 at.% for PO-SC, while 2.77 at.% P was introduced, indicating the successful doping of P and O into the carbon. Higher amount of NaH_2PO_4 would generally lead to higher P and O, while the amount of P in PO-SC and PO-SC-19 are both 2.77 at.% without further increase (Table S3). The secondary carbonization obviously reduces the contents of O and P to 4.79 and 1.71 at.%, respectively for PO-SC-S, which are further decreasing in the PO-SC-S1000 at higher temperature. The elemental analysis also indicates the similar trend that the contents of P and O increase with the increasing amounts of NaH_2PO_4 but decrease upon secondary carbonization (Table S4). It is widely proved that the heteroatom doping such as P and O can effectively enhance the capacity but meanwhile reduce the ICE.^[19,27,47] This is also in well accordance with our cases that higher amount of P/O doping leads to continuously improved specific capacities from 194 for SC to 263 mAh g^{-1} for PO-SC-19, but reduced ICE from 80% to 60%. However, upon secondary carbonization, both the P and O significantly decreased for PO-SC-S, but the capacity is almost unchanged (249 mAh g^{-1}) with recovered ICE to 80% compared to PO-SC (Figure 3a, Table S1 and S3). This suggests that the electrochemical performance is not simply affected by the doping amount of heteroatoms, but more likely the specific heteroatom configurations.

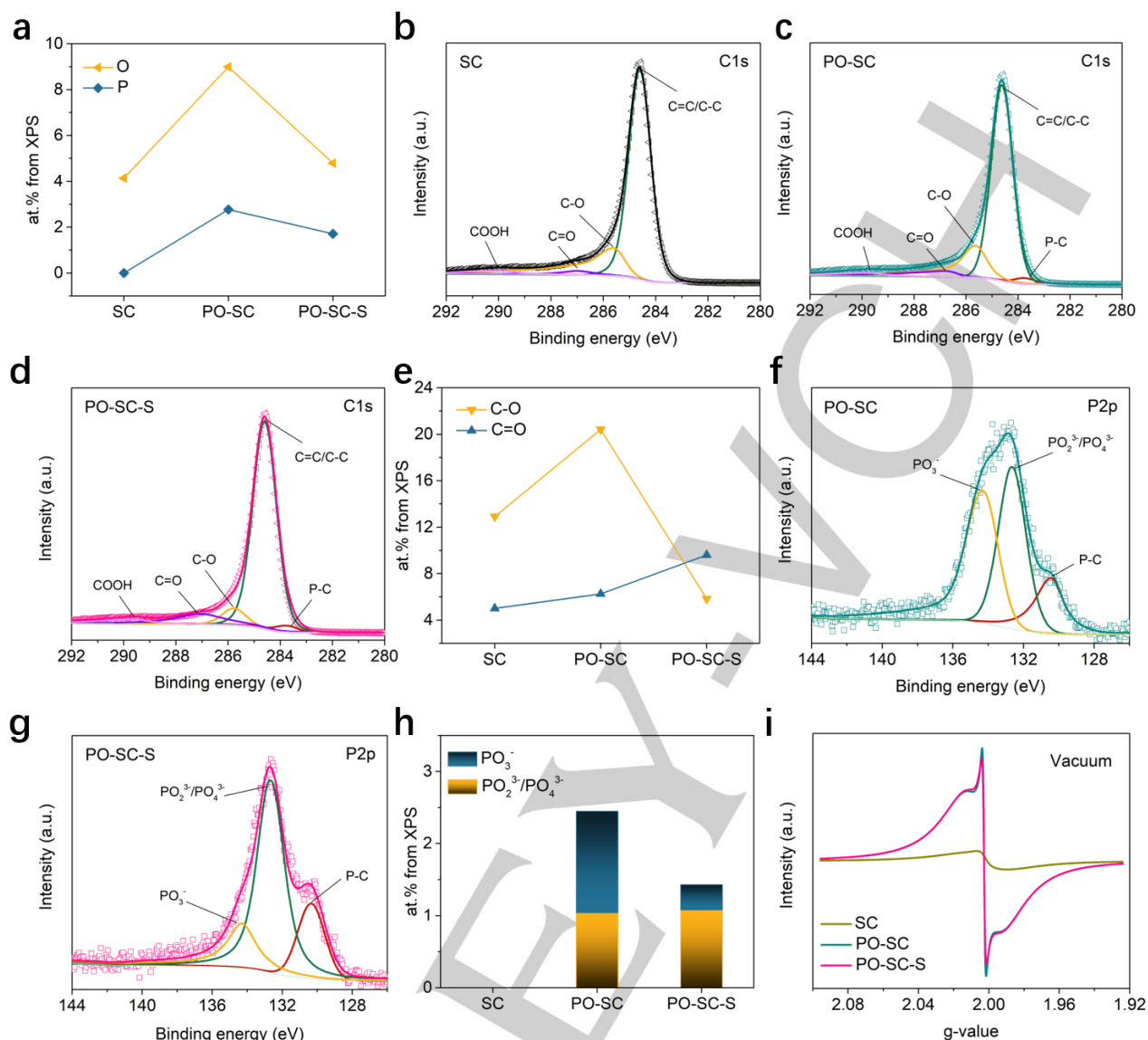


Figure 3. (a) Comparison of the O and P percentages between SC, PO-SC and PO-SC-S based on XPS survey. (b-d) Fitted XPS C1s spectra of SC, PO-SC and PO-SC-S. (e) Comparison of the C-O and C=O percentages between SC, PO-SC and PO-SC-S based on the XPS C1s fittings. (f-g) Fitted XPS P2p spectra of PO-SC and PO-SC-S. (h) Comparison of the PO₂³⁻/PO₄³⁻ and PO₃⁻ configurations between PO-SC and PO-SC-S based on the XPS P2p fittings. (i) EPR spectra of SC, PO-SC and PO-SC-S under vacuum.

Then heteroatom configurations are carefully analyzed by further studying the XPS results. The C1s spectra of the resulting samples are shown in Figure 3b-d and Figure S10. Five peaks centered at around 283.8, 284.6, 285.7, 287.0 and 289.8 eV correspond to C-P, C=C/C-C, C-O, C=O and COOH, respectively.^[8] It is approved before that both C-O and C=O can enhance the Na storage performance, but C=O can contribute more reversible Na adsorption while C-O incline leads to much irreversibility.^[20,21] As shown in Figure 3e and Table S3, the P/O doping slightly increases the amount of C=O from 5.00 at.% in SC to 5.41 at.% in PO-SC, and strongly increases C-O from 12.91 to 17.66 at.%. Yet, the secondary carbonization further increases the C=O to 9.6 at.%, while sharply decreases the C-O to 5.82 at.% for PO-SC-S. Herein, it is clearly that the increasing ratio of NaH₂PO₄ increases both C=O and C-O amount, but the increase of C-O is more obvious to cause continuously reduced ICE. The secondary carbonization can further increase the C=O to provide more reversible capacity, and meanwhile suppress the irreversibility by the diminishment of C-O. To be noted,

higher carbonization temperature of 1000°C decreases the amount of C=O while significantly increases C-O, which leads to lower ICE for PO-SC-S1000.

Similarly, the P2p spectra shown in Figure 3f-g and Figure S11 are deconvoluted to three peaks at around 130.3, 132.6 and 134.3 eV, corresponding to P-C, hypophosphate/phosphate (PO₂³⁻/PO₄³⁻), and metaphosphate (PO₃⁻), respectively.^[48-50] The P-C continuously reduces, while PO₂³⁻/PO₄³⁻ and PO₃⁻ enhance with the increasing ratio of NaH₂PO₄ (Table S3), which is consistent with the fact that P prefers to be doped with O as PO_x type in carbon when using the O-containing P precursors.^[19,51] Interestingly, after the secondary carbonization, the PO₃⁻ group significantly reduces to 0.35 at.% in PO-SC-S from 1.41 at.% in PO-SC, instead, the PO₂³⁻/PO₄³⁻ further slightly increases from 1.04 to 1.08 at.% (Figure 3h). Correlating with the similar reversible capacity and improved ICE of PO-SC and PO-SC-S, it is implied that the increase of PO₂³⁻/PO₄³⁻ and decrease of PO₃⁻ after

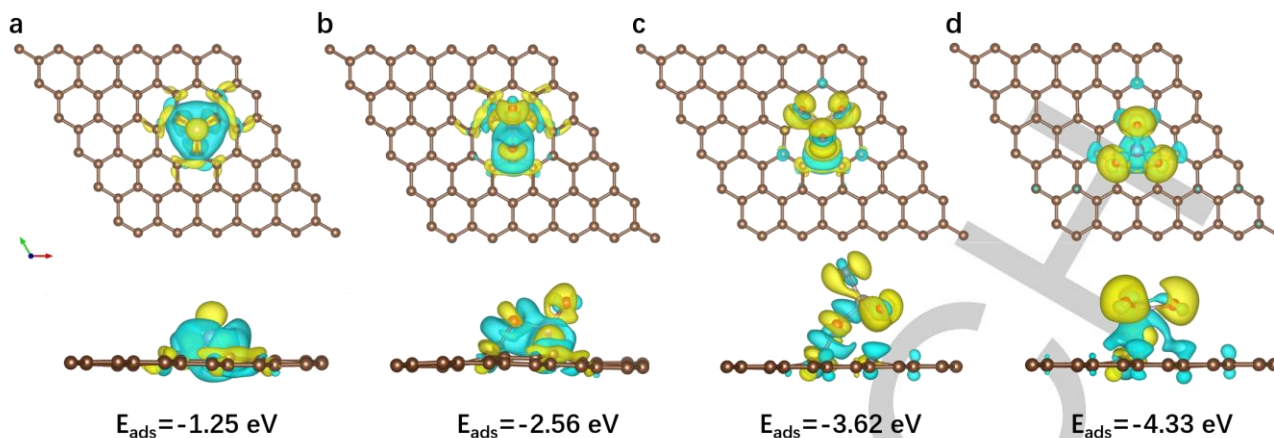


Figure 4. Charge distribution of (a) P, (b) PO_2 , (c) PO_4 and (d) PO_3 configurations in the carbons at top (top) and side (bottom) views with the corresponding adsorption energy of Na^+ ions.

secondary carbonization contribute to the retaining of the sloping capacity and the recovery of ICE.

The first principle calculations were carried out to further verify the effects of the P-based configurations. Figure 4 shows the differential charge density (DCD) maps of single P, PO_2 , PO_4 and PO_3 configurations, respectively. It is obvious that the positive charged regions (blue) are preferred to be accumulated around the P atoms, while the negative charged regions (yellow) with excess electrons are preferred to be around the O atoms, which is beneficial to the adsorption of Na^+ ions. The Bader charges of the P atom in the single-P configuration are +1.7, but around +3.2 for all the PO_x configurations, which also confirms that the existence of O can obtain more electrons from P and even surrounding C atoms due to the strong electronegativity. The adsorption energy of Na on pure carbon is only -0.64 eV but improves to -1.25 eV on a single-P configuration. The energy could further increase to -2.56 and -3.62 eV for PO_2 and PO_4 , respectively, and even as high as -4.33 eV for PO_3 . This is consistent with the experimental results that the $\text{PO}_2^{3-}/\text{PO}_4^{3-}$ and PO_3^- can effectively enhance the Na storage capacity compared to the undoped carbon and the P-C configuration. However, much higher adsorption energy of PO_3^- also means more difficult desorption of Na^+ ions, leading to strong irreversibility and lower ICE.

Moreover, it is also found that the free radicals in the “slope-dominated” carbons are closely related to the heteroatoms doping and secondary carbonization according to the electron paramagnetic resonance (EPR) tests. The measurements were performed under vacuum to diminish the influence of the adsorbed oxygen molecules with the dangling bonds.^[41] As shown in Figure 3i and Figure S14, the EPR signals of the P/O-doped carbons present a pair of narrow sharp peaks with small peak-to-peak line width (ΔH_{pp}) and a pair of broader peaks with larger ΔH_{pp} , which correspond to the dangling bonds or terminated free radicals from the lone-pair electrons and the free charge carriers, respectively.^[41,52–54] In the contrary, the SC shows significantly weak EPR signals, indicating limited free radicals. The P/O doping significantly improves contents of free radicals as well as free charge carriers, facilitating the Na storage capabilities. The content of such atomic groups undergo almost no change after secondary carbonization, which is also an important reason for the constant of sloping capacity between PO-SC and PO-SC-S, while the reduction of such radical

configuration upon higher carbonization temperature decreases the Na storage performance for PO-SC-S1000 (Figure S14b).

In short, although the absolute amount of P and O decreases after the secondary carbonization, this process helps screen the heteroatom configurations: the decreased C-O and PO_3^- and increased C=O and $\text{PO}_2^{3-}/\text{PO}_4^{3-}$, as well as the retained free radicals synergistically contribute to the high sloping capacity and ICE. These results inspire that the absolute heteroatom doping degree is not the most important point as most previous works pursued, while the focus on specific heteroatom configurations can contribute more on the practical reversible sloping capacity. This could be easily achieved by screening the configurations (i.e. secondary thermal treatment), but some other strategies may also be feasible to further enhance the reversible sloping capacity, which desires future exploration.

To further study the Na storage mechanisms of the obtained “slope-dominated” carbons optimized by the heteroatom configurations screening, the cyclic voltammetry (CV) was first performed to see the electrochemical behavior within the potential window. As shown in Figure 5a-c, there are pairs of sharp redox peaks at around 0.1 V (vs. Na^+/Na), which is similar to the typical CV curves of carbon anodes containing plateaus. Moreover, the b -value in $i = aU^b$ ^[55] of this peak, fitted based on the different scan rates of CV, is 0.569 for SC during the reduction process (Figure S15 and Figure 5d-f), meaning a diffusion-controlled process just like normal hard carbons with plateaus. The P/O doping slightly increases the b -value to 0.672 for PO-SC but decreases back to 0.576 for PO-SC-S, which suggests that some surface-controlled pseudocapacitive reactions with Na^+ ions may occur at the low-potential region, but diminished upon the heteroatom configuration screening process (the relatively higher b -values at oxidation process indicate slight asymmetry of the sodiation and desodiation procedures). Thus, the “slope-dominated” carbons not only have adsorption or pseudocapacitive interactions with the Na^+ ions on the surface as commonly thought, but also deliver diffusion-controlled redox reactions at low-potential regions, which may have similar Na storage mechanism to that of the normal carbons with plateaus. Comparing the 2nd cycle-sodiation capacity of SC, PO-SC and PO-SC-S (Figure 5g), it is found that the capacities below 0.1 V (vs. Na^+/Na) are almost the same, while the capacity enhancement resulted from the P/O doping is majorly from the high-potential regions above 0.1 V (vs. Na^+/Na), meaning that

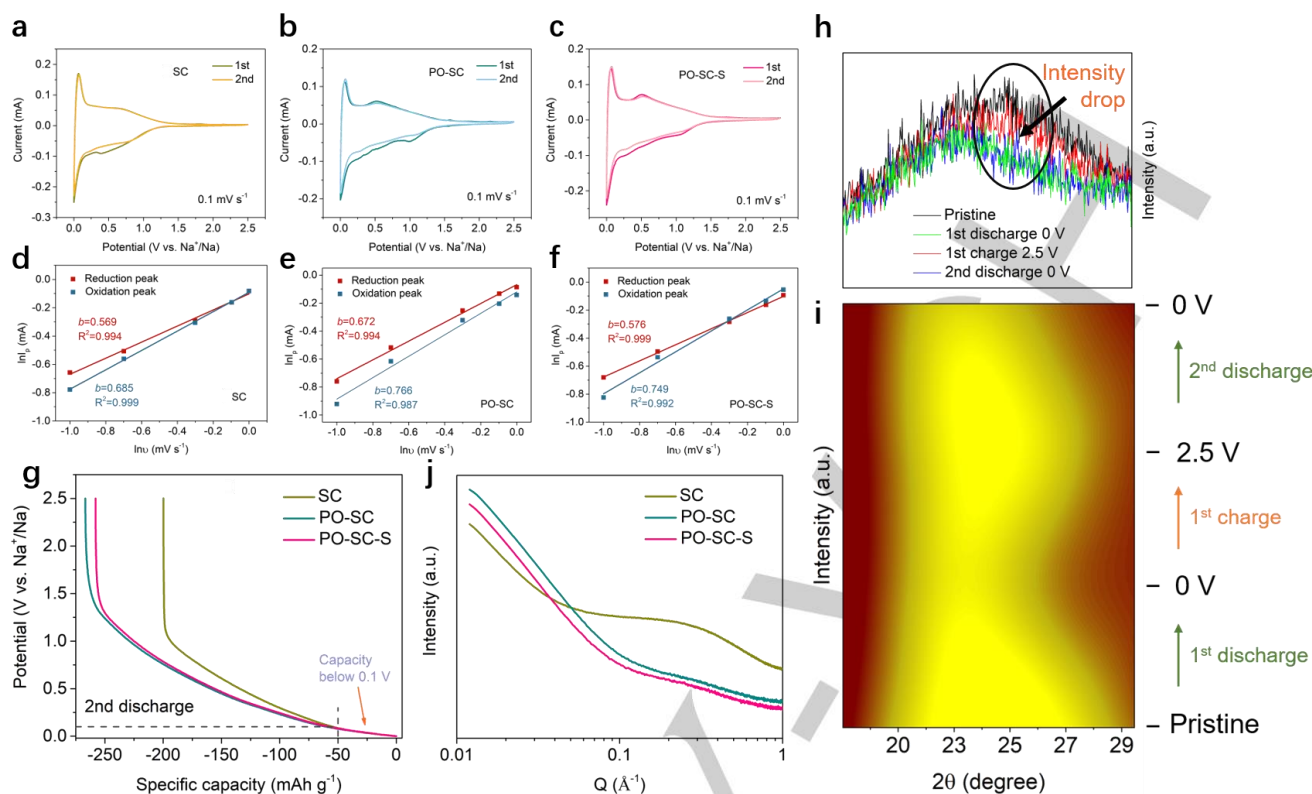


Figure 5. (a-c) First- and second-cycle CV curves of SC, PO-SC and PO-SC-S at 0.1 mV s⁻¹, respectively. (d-f) Fitted b-values of SC, PO-SC and PO-SC-S, respectively based on the CV. (g) 2nd discharge curves of SC, PO-SC and PO-SC-S, respectively. (h-i) (002) peaks from the in situ XRD patterns of PO-SC-S. (j) SAXS profiles of SC, PO-SC and PO-SC-S, respectively.

the introduced and screened heteroatom configurations together with the defects and free radicals mainly contribute to the surface-controlled Na adsorption, which is accord with the common knowledge.

Then a question comes out that what is the mechanism at the low-potential region without obvious plateau? Many reports proposed the occurrence of intercalation behavior of Na⁺ ions into the graphitic layers,^[31,56,57] to clarify this, the in situ XRD was performed for PO-SC-S. Figure S16 shows typical in situ XRD profiles at various states of sodiation/desodiation. It seems like that the (002) peaks undergo shift towards lower angles during the sodiation and can reversibly shift back upon desodiation. Nevertheless, looking carefully at the (002) peaks shown in Figure 5h-i, there is actually no position shift, which implies no intercalation, but the intensities of the peaks decrease during the sodiation and recover upon desodiation. It is worth noting that due to the large width of the peak, the intensity varies in different regions, particularly, the signal significantly reduces at the relative higher-angle region representing smaller *d*-spacing compared to the lower-angle region with larger *d*-spacing. This is because the out-of-phase scattering and destructive interference caused by the diffusion of Na close to graphene layers normally lead to the intensity drop.^[58] The destructive interference is stronger in smaller *d*-spacing areas, which makes intensity drop more obvious at higher diffraction angles. This could also somewhat explain the different conclusions in literatures obtained according to the in situ XRD analysis:^[58-61] the carbon anodes with relatively small average *d*-spacing experiencing strong peak intensity drop at higher-angle region, looking like that the average peak position shifts to lower angles. However, if the carbon anode has relatively larger average *d*-

spacing so that the peak position mainly locates at the lower angles, the intensity drop will not be obvious, and the average peak position will seem unchanged.

Besides, small angle X-ray scattering (SAXS) patterns of SC, PO-SC and PO-SC-S were also obtained to observe the pore structures, whose shoulders with broad convex shape at the range of $Q=0.1-1 \text{ \AA}^{-1}$ indicate the existence of some nanopores. It can be seen in Figure 5j that the shoulders become flatter and the intensities decrease for PO-SC and PO-SC-S. Fitting the SAXS patterns using the Porod method (Figure S17),^[8,45,62,63] the B_2 factors proportional to the pore numbers are 9.65, 5.87 and 5.88 for SC, PO-SC and PO-SC-S, respectively, while the diameters of nanopores are calculated as small as 0.79 nm for SC and even smaller of 0.65 and 0.62 nm for PO-SC and PO-SC-S, respectively (Table S5), meaning both pore number and pore size are reduced upon the P/O doping and secondary carbonization.^[8,45,64,65] These suggest that the low-potential regions are still considered to be attributed to the nanopore filling, however, the too small pore sizes may be the major influence that are unsatisfied for Na⁺ ions to accommodate since the filled Na clusters in the pore to form plateau are proposed to be around 1.3-1.5 nm. Although the pore numbers have differences before and after P/O doping that should have led to different plateau capacities,^[66] the improper pore size results in the similar and unexploited capacities at the low-potential regions as well as the absence of plateau.

In a word, the resulting "slope-dominated" carbon anodes with screened heteroatom configurations was used as a model material to investigate the Na storage mechanism from a new and opposite point of view based on the nature of the absence of plateau. It is found that the enhanced reversible sloping

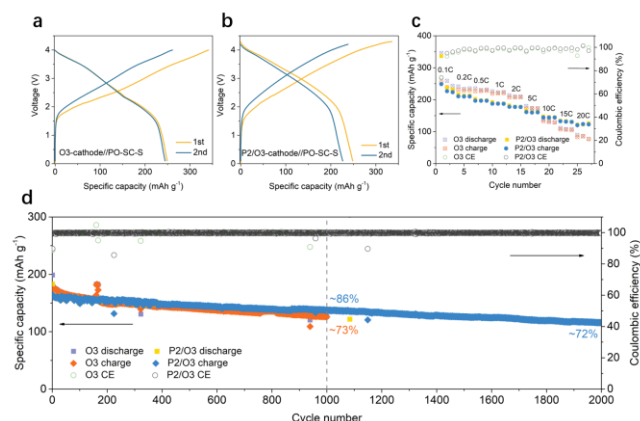


Figure 6. (a-b) Galvanostatic charge/discharge curves at the first and second cycles of the full cells with PO-SC-S anode and O₃- or biphasic P₂/O₃-type cathode at 0.1C. (c) Rate performance of the full cells with PO-SC-S anode and O₃- or P₂/O₃-type cathode from 0.1 to 20C. (d) Cycling stability of the full cells with PO-SC-S anode and O₃- or P₂/O₃-type cathode at 3C. The current rates are based on the cathodes.

capacity from the introduced and filtered heteroatoms still contribute to the range of above 0.1 V (vs. Na⁺/Na). The low-potential region is also a diffusion-controlled redox behavior, which is due to the nanopore filling, but the too small pore size leads to the absence of plateau. Thus, engineering proper heteroatom configurations with smaller nanopore size would be an effective way to make the “slope-dominated” carbon anodes.

Finally, to evaluate the practical performance of the “slope-dominated” carbon anodes, PO-SC-S was paired with O₃- and biphasic P₂/O₃-type transition metal layered oxide cathodes, respectively. The full cells can both deliver high capacity of ~250 mAh g⁻¹ (based on anode) with the energy densities of 205 and 218 Wh kg⁻¹ (based on both cathode and anode), respectively at 0.1C (Figure 6a-b) and exhibit good rate capability (Figure 6c). The full cell presents higher capacities until 5C (180 mAh g⁻¹) with O₃-type cathode, and superior capability even at 20C (124 mAh g⁻¹) with the P₂/O₃-type cathode. Moreover, the cycling stability of the full cell with P₂/O₃-type cathode is better than that with O₃-type cathode, demonstrating ~86% and 73% capacity retention at 3C after 1000 cycles, respectively, and the former still possesses ~72% capacity retention after 2000 cycles (Figure 6d). This suggests that optimizing the full cell system such as using different cathodes can adjust to achieve high rate and cycling performance, promising the great potential of the practical “slope-dominated” carbon anodes for high-power NIBs.

Conclusion

The “slope-dominated” carbon anode materials with the simultaneity between high sloping capacity and high ICE were successfully developed owing from the secondary carbonization process after P/O doping. We found that the type of heteroatom configurations is much more important than the doping amount, where the secondary carbonization can screen the C-O and PO₃⁻ configurations with more irreversible capacity and improve the more reversible C=O and PO₂³⁻/PO₄³⁻ configurations as well as retaining the free radicals. Furthermore, the systematically studied Na storage mechanisms of the obtained “slope-dominated” carbons revealed that the diffusion-controlled process also exists at the low-potential region, while the too small nanopores cause the absence of the plateau. By pairing

with different cathodes, the full cells can be optimized to deliver superior rate and cycling performance. This work may inspire to distinguish and screen the heteroatom configurations for fast and reversible Na storage and promises the future design of practical “slope-dominated” carbon anodes toward high-power NIBs.

Acknowledgements

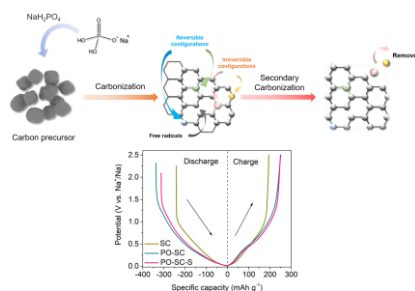
This work was supported by the National Natural Science Foundation (NSFC) of China (51725206 and 52072403), NSFC-UKRI_EPSRC (51861165201), the Strategic Priority Research Program of the Chinese Academy of Sciences (XDA21070500), Youth Innovation Promotion Association of the Chinese Academy of Sciences (2020006), China Postdoctoral Science Foundation funded Project (2021M693367) and Beijing Municipal Natural Science Foundation (2212022). Z. Guo and Z. Xu thank the China Scholarship Council for the PhD funding.

Keywords: Heteroatom configurations, sloping capacity, ICE, high-power NIBs

- [1] B. Dunn, H. Kamath, J. M. Tarascon, *Science* **2011**, *334*, 928–935.
- [2] C. Zhao, Q. Wang, Z. Yao, J. Wang, B. Sánchez-Lengeling, F. Ding, X. Qi, Y. Lu, X. Bai, B. Li, H. Li, A. Aspuru-Guzik, X. Huang, C. Delmas, M. Wagemaker, L. Chen, Y. S. Hu, *Science* **2020**, *370*, 708–712.
- [3] R. Usiskin, Y. Lu, J. Popovic, M. Law, P. Balaya, Y.-S. Hu, J. Maier, *Nat. Rev. Mater.* **2021**, *6*, 1020-1035.
- [4] P. K. Nayak, L. Yang, W. Brehm, P. Adelhelm, *Angew. Chemie - Int. Ed.* **2018**, *57*, 102–120.
- [5] C. Zhao, Q. Wang, Y. Lu, B. Li, L. Chen, Y. S. Hu, *Sci. Bull.* **2018**, *63*, 1125–1129.
- [6] Q. Meng, Y. Lu, F. Ding, Q. Zhang, L. Chen, Y. S. Hu, *ACS Energy Lett.* **2019**, *4*, 2608–2612.
- [7] A. Kamiyama, K. Kubota, D. Igarashi, Y. Youn, Y. Tateyama, H. Ando, K. Gotoh, S. Komaba, *Angew. Chemie - Int. Ed.* **2020**, *60*, 5114–5120.
- [8] F. Xie, Z. Xu, A. Jensen, F. Ding, H. Au, J. Feng, H. Luo, M. Qiao, Z. Guo, Y. Lu, A. Drew, Y.-S. Hu, M. Titirici, *J. Mater. Chem. A* **2019**, *7*, 27567–27575.
- [9] Y. Li, Y. Lu, Q. Meng, A. C. S. Jensen, Q. Zhang, Q. Zhang, Y. Tong, Y. Qi, L. Gu, M.-M. Titirici, Y. Hu, *Adv. Energy Mater.* **2019**, 1902852.
- [10] C. Choi, D. S. Ashby, D. M. Butts, R. H. DeBlock, Q. Wei, J. Lau, B. Dunn, *Nat. Rev. Mater.* **2020**, *5*, 5-19.
- [11] S. Li, J. Qiu, C. Lai, M. Ling, H. Zhao, S. Zhang, *Nano Energy* **2015**, *12*, 224–230.
- [12] F. Xie, Z. Xu, Z. Guo, M. Titirici, *Prog. Energy* **2020**, *2*, 042002.
- [13] F. Xie, Z. Xu, Z. Guo, Y. Lu, L. Chen, M.-M. Titirici, Y.-S. Hu, *Sci. China Chem.* **2021**, *64*, 1679-1692.
- [14] W. Chen, M. Wan, Q. Liu, X. Xiong, F. Yu, Y. Huang, *Small Methods* **2019**, *3*, 1800323.
- [15] Y. Li, M. Chen, B. Liu, Y. Zhang, X. Liang, X. Xia, *Adv. Energy Mater.* **2020**, *10*, 2000927.
- [16] B. Cao, H. Liu, B. Xu, Y. Lei, X. Chen, H. Song, *J. Mater. Chem. A* **2016**, *4*, 6472–6478.
- [17] Q. Jin, K. Wang, P. Feng, Z. Zhang, S. Cheng, K. Jiang, *Energy Storage Mater.* **2020**, *27*, 43–50.
- [18] R. Guo, C. Lv, W. Xu, J. Sun, Y. Zhu, X. Yang, J. Li, J. Sun, L. Zhang, D. Yang, *Adv. Energy Mater.* **2020**, *10*, 1903652.
- [19] Z. Li, L. Ma, T. W. Surta, C. Bommier, Z. Jian, Z. Xing, W. F. Stickle, M. Dolgos, K. Amine, J. Lu, T. Wu, X. Ji, *ACS Energy Lett.* **2016**, *1*, 395–401.

- [20] C. Zhou, A. Li, B. Cao, X. Chen, M. Jia, H. Song, *J. Electrochem. Soc.* **2018**, *165*, A1447–A1454.
- [21] C. Chen, Y. Huang, Y. Zhu, Z. Zhang, Z. Guang, Z. Meng, P. Liu, *ACS Sustain. Chem. Eng.* **2020**, *8*, 1497–1506.
- [22] H. Yang, R. Xu, Y. Yu, *Energy Storage Mater.* **2019**, *22*, 105–112.
- [23] J. Zhang, D. W. Wang, W. Lv, S. Zhang, Q. Liang, D. Zheng, F. Kang, Q. H. Yang, *Energy Environ. Sci.* **2017**, *10*, 370–376.
- [24] Y. Zhen, R. Sa, K. Zhou, L. Ding, Y. Chen, S. Mathur, Z. Hong, *Nano Energy* **2020**, *74*, 104895.
- [25] J. Tan, J. Matz, P. Dong, J. Shen, M. Ye, *Adv. Energy Mater.* **2021**, 2100046.
- [26] Y. Qi, Y. Lu, F. Ding, Q. Zhang, H. Li, X. Huang, L. Chen, Y. Hu, *Angew. Chemie - Int. Ed.* **2019**, *131*, 4405–4409.
- [27] K. L. Hong, L. Qie, R. Zeng, Z. Q. Yi, W. Zhang, D. Wang, W. Yin, C. Wu, Q. J. Fan, W. X. Zhang, Y. H. Huang, *J. Mater. Chem. A* **2014**, *2*, 12733–12738.
- [28] N. Li, Q. Yang, Y. Wei, R. Rao, Y. Wang, M. Sha, X. Ma, L. Wang, Y. Qian, *J. Mater. Chem. A* **2020**, *8*, 20486–20492.
- [29] L. Xiao, H. Lu, Y. Fang, M. L. Sushko, Y. Cao, X. Ai, H. Yang, J. Liu, *Adv. Energy Mater.* **2018**, *8*, 1703238.
- [30] J. Liu, Y. Zhang, L. Zhang, F. Xie, A. Vasileff, S. Z. Qiao, *Adv. Mater.* **2019**, *31*, 1901261.
- [31] W. Luo, Z. Jian, Z. Xing, W. Wang, C. Bommier, M. M. Lerner, X. Ji, *ACS Cent. Sci.* **2015**, *1*, 516–522.
- [32] N. Wang, Y. Wang, X. Xu, T. Liao, Y. Du, Z. Bai, S. Dou, *ACS Appl. Mater. Interfaces* **2018**, *10*, 9353–9361.
- [33] D. Li, L. Zhang, H. Chen, L. Ding, S. Wang, H. Wang, *Chem. Commun.* **2015**, *51*, 16045–16048.
- [34] K. Tang, L. Fu, R. J. White, L. Yu, M. Titirici, M. Antonietti, J. Maier, *Adv. Energy Mater.* **2012**, *2*, 873–877.
- [35] Y. S. Yun, K. Y. Park, B. Lee, S. Y. Cho, Y. U. Park, S. J. Hong, B. H. Kim, H. Gwon, H. Kim, S. Lee, Y. W. Park, H. J. Jin, K. Kang, *Adv. Mater.* **2015**, *27*, 6914–6921.
- [36] J. Zhu, C. Chen, Y. Lu, Y. Ge, H. Jiang, K. Fu, X. Zhang, *Carbon* **2015**, *94*, 189–195.
- [37] X. Yao, Y. Ke, W. Ren, X. Wang, F. Xiong, W. Yang, M. Qin, Q. Li, L. Mai, *Adv. Energy Mater.* **2019**, *9*, 1803260.
- [38] Z. Xu, F. Xie, J. Wang, H. Au, M. Tebyetekerwa, Z. Guo, S. Yang, Y. S. Hu, M. M. Titirici, *Adv. Funct. Mater.* **2019**, *29*, 1903895.
- [39] L. Xiao, Y. Cao, W. A. Henderson, M. L. Sushko, Y. Shao, J. Xiao, W. Wang, M. H. Engelhard, Z. Nie, J. Liu, *Nano Energy* **2016**, *19*, 279–288.
- [40] H. Lu, X. Chen, Y. Jia, H. Chen, Y. Wang, X. Ai, H. Yang, Y. Cao, *Nano Energy* **2019**, *64*, 103903.
- [41] K. Kubota, S. Shimadzu, N. Yabuuchi, S. Tominaka, S. Shiraiishi, M. Abreu-Sepulveda, A. Manivannan, K. Gotoh, M. Fukunishi, M. Dahbi, S. Komaba, *Chem. Mater.* **2020**, *32*, 2961–2977.
- [42] A. C. Ferrari, J. Robertson, *Phys. Rev. B* **2000**, *61*, 14095–14107.
- [43] A. C. Ferrari, J. Robertson, *Philos. Trans. R. Soc. A Math. Phys. Eng. Sci.* **2004**, *362*, 2477–2512.
- [44] A. C. Ferrari, D. M. Basko, *Nat. Nanotechnol.* **2013**, *8*, 235–246.
- [45] F. Xie, Z. Xu, A. C. S. Jensen, H. Au, Y. Lu, V. Araullo-Peters, A. J. Drew, Y.-S. Hu, M.-M. Titirici, *Adv. Funct. Mater.* **2019**, *29*, 1901072.
- [46] Z. Xu, Z. Guo, R. Madhu, F. Xie, R. Chen, J. Wang, M. Tebyetekerwa, Y.-S. Hu, M. Titirici, *Energy Environ. Sci.* **2021**, *14*, 6381–6393.
- [47] H. Hou, L. Shao, Y. Zhang, G. Zou, J. Chen, X. Ji, *Adv. Sci.* **2017**, *4*, 1600243.
- [48] A. V. Naumkin, C. Kraut-Vass, A. Gaarenstroom, S. W. Powell J., “NIST X-ray Photoelectron Spectroscopy Database, Version 4.1,” can be found under <https://srdata.nist.gov/xps/>, **2012**.
- [49] A. M. Puziy, O. I. Poddubnaya, R. P. Socha, J. Gurgul, M. Wisniewski, *Carbon* **2008**, *46*, 2113–2123.
- [50] Y. Wen, B. Wang, C. Huang, L. Wang, D. Hulicova-Jurcakova, *Chem. - A Eur. J.* **2015**, *21*, 80–85.
- [51] J. Yan, H. Li, K. Wang, Q. Jin, C. Lai, R. Wang, S. Cao, J. Han, Z. Zhang, J. Su, K. Jiang, *Adv. Energy Mater.* **2021**, 2003911.
- [52] F. G. Emmerich, C. Rettori, C. A. Luengo, *Carbon* **1991**, *29*, 305–311.
- [53] S. L. Vittorio, A. Nakayama, T. Enoki, M. S. Dresselhaus, M. Endo, N. Shindo, *J. Mater. Res.* **1993**, *8*, 2282–2287.
- [54] L. Zhang, W. He, K. Shen, Y. Liu, S. Guo, *J. Alloys Compd.* **2018**, *760*, 84–90.
- [55] P. Lu, Y. Sun, H. Xiang, X. Liang, Y. Yu, *Adv. Energy Mater.* **2017**, *8*, 1702434.
- [56] E. Buiel, J. R. Dahn, *Electrochim. Acta* **1999**, *45*, 121–130.
- [57] Z. Jian, C. Bommier, L. Luo, Z. Li, W. Wang, C. Wang, P. A. Greaney, X. Ji, *Chem. Mater.* **2017**, *29*, 2314–2320.
- [58] D. A. Stevens, J. R. Dahn, *J. Electrochem. Soc.* **2001**, *148*, 803–811.
- [59] C. Bommier, T. W. Surta, M. Dolgos, X. Ji, *Nano Lett.* **2015**, *15*, 5888–5892.
- [60] Y. Li, Y. S. Hu, M. M. Titirici, L. Chen, X. Huang, *Adv. Energy Mater.* **2016**, *6*, 1600659.
- [61] B. Zhang, C. M. Ghimbeu, C. Laberty, C. Vix-Guterl, J. M. Tarascon, *Adv. Energy Mater.* **2016**, *6*, 1501588.
- [62] H. Au, H. Alptekin, A. C. S. Jensen, E. Olsson, C. A. O’Keefe, T. Smith, M. Crespo-Ribadeneyra, T. F. Headen, C. P. Grey, Q. Cai, A. J. Drew, M.-M. Titirici, *Energy Environ. Sci.* **2020**, *13*, 3469–3479.
- [63] D. A. Stevens, J. R. Dahn, *J. Electrochem. Soc.* **2000**, *147*, 4428–4431.
- [64] A. J. Smith, M. J. MacDonald, L. D. Ellis, M. N. Obrovac, J. R. Dahn, *Carbon* **2012**, *50*, 3717–3723.
- [65] V. Simone, A. Boulineau, A. de Geyer, D. Rouchon, L. Simonin, S. Martinet, *J. Energy Chem.* **2016**, *25*, 761–768.
- [66] J. M. Stratford, A. K. Kleppe, D. S. Keeble, P. A. Chater, S. S. Meysami, C. J. Wright, J. Barker, M. Titirici, P. K. Allan, C. P. Grey, *J. Am. Chem. Soc.* **2021**, *143*, 14274–14286.

Entry for the Table of Contents



Using a heteroatom configuration screening strategy upon P/O-doping, irreversible configurations of C-O and PO_3^- were removed, while the configurations like C=O and $\text{PO}_4^{3-}/\text{PO}_2^{3-}$ as well as the free radicals could be retained or even enhanced. The Na storage mechanisms were also studied using the resulting carbon. This work inspires the design and understanding of the “slope-dominated” carbon anodes towards high-power Na-ion batteries.